Turnbull, R.E., et al., 2021, A hidden Rodinian lithospheric keel beneath Zealandia, Earth's newly recognized continent: Geology, v. 49, https://doi.org/10.1130/G48711.1

SUPPLEMENTAL MATERIAL

Methods

In situ O-Hf-U-Pb isotopic analyses were undertaken on existing zircon separates for which U-Pb ages have been published (n = 131; see Table S5 in supplementary material) (Kimbrough et al. 1994; Muir et al. 1996, 1997, 1998; Ramezani and Tulloch 2009; Tulloch et al. 2009, 2011; Allibone et al. 2016a,b; Sagar et al. 2016; Turnbull et al. 2016; Buritica et al. 2019; Ringwood et al. submitted), or from mineral separates made on new samples collected during this research (n = 38). Location information for all samples analysed can be found Table S5 and in the online Petlab database (Strong et al. 2016; http://pet.gns.cri.nz) or requested from the authors. Where new zircon separates were obtained, zircon separation was undertaken at GNS Science using standard crushing, heavy liquid and magnetic separation techniques. Together with the two zircon standard reference materials 91500 (Wiedenbeck et al. 2004) and TEMORA 2 (Black et al. 2004), zircon crystals were handpicked and mounted in epoxy. All zircon grains were mounted within 8 mm of the centre of a 1-inch mount, and extra care was taken to ensure a smooth, flat, low-relief polish (Kita et al. 2009). Zircon were imaged by Scanning Electron Microscope (SEM) – cathodoluminescence (CL) at California State University Northridge (CSUN) and Otago University, New Zealand to reveal internal complexity and aid in the selection of analytical spot locations (Supplementary Fig. 1). All O-isotopic analyses were performed first, followed by split-stream Lu-Hf-U-Pb analyses over the same analytical spot as the previous O-isotope analysis. All samples analysed have well established U-Pb zircon crystallization ages from published and unpublished data – U-Pb results for all Lu-Hf spots were used to ensure the domain of zircon analysed was representative of the magmatic crystallization age, rather than an older inherited domain, or a younger domain affected by Pb-loss or metamorphic recrystallization.

O-Isotope Analyses

All O-isotope analyses for this study were measured by secondary ion mass spectrometry (SIMS) at the Institut für Geowissenschaften, Universität Heidelberg, using a CAMECA IMS 1280-HR ion microprobe. Data for all analyses (unknowns) are available in Supplementary Table S1. All zircon mounts were gold coated prior to O-isotope analyses. A 2 nA, 20 keV Cs^+ primary ion beam with a raster size of 10 µm (12 µm during pre-sputtering) was used, resulting in an analytical spot size of ~ 15 x 15 µm, and depths of ~1 µm. Negative secondary ions were accelerated to 10 keV. The secondary ion image was limited to 30 µm, the dynamic transfer optical system (DTOS) was activated and sample charging was compensated with the normal incidence electron gun (NEG). ^{16}O and ^{18}O were detected simultaneously in two Faraday cups. The nominal mass resolving power for ^{16}O and ^{18}O was 2500. Including the time for beam centering the analyses started after a total pre-sputtering time of ~80 s and each analysis comprised 20 cycles with 4 s integration time per cycle. The internal uncertainty reported is the relative standard deviation of the mean value of the isotope ratios. The baseline of the FC amplifiers was determined separately with an integration time of 200 s several times per session. All $\delta^{18}O$ values are reported relative to Vienna Standard Mean Ocean Water (VSMOW). For all but one sample the primary standard used was 91500 zircon (Wiedenbeck et al. 2004), with TEMORA 2 zircon (Black et al. 2004) as the secondary standard. The mean repeatability of the 91500 calibrations was 0.09 ‰ (0.04 ‰ – 0.16 ‰, 1 std. dev [1sd]). The mean value of 267 TEMORA 2 analyses was $\delta^{18}O$ = +8.04 ‰ ± 0.15 ‰ (1sd) equal to the published values of +8.2 ± 0.1 ‰ within uncertainty (Black et al. 2004). For one sample, KIM-5 zircon (Peck et al. 2001) was used as primary standard with a repeatability of 0.08 ‰ (1sd). For this sample, the result for TEMORA 2 was $\delta^{18}O$ = +8.19 ‰ ± 0.15 ‰ (1sd). All data for the standards used for O-isotope analysis are presented in Supplementary Table S3. Internal measurement uncertainties for individual analyses were typically ≤ 0.1 ‰ (1 standard error of the mean ratio), and within sample variation was typically < 0.4 ‰. Analyses were made concurrently over the course of 13 days.

Lu-Hf and U-Pb Analyses

All new Lu-Hf and U-Pb isotopic analyses (Supplementary Table S2) were simultaneously obtained by laser ablation split stream over 12 days at the Geohistory Facility in the John de Laeter Centre, Curtin University using protocols described in Spencer et al. (2017). Zircon crystals were ablated using a Resonetics RESOlution M-50A incorporating a Compex 102 excimer laser, coupled to a Nu Plasma II multi-collector inductively coupled plasma mass spectrometer (MC-ICPMS) for Lu-Hf isotope determination and an Agilent 7700 quadrupole inductively coupled plasma mass spectrometer (Q-ICP-MS) for age (U-Pb) and trace element determination. Mounts were gently hand polished before Hf-isotope analyses to ensure the O-isotope analytical spot was no longer visible. Each analytical spot was placed directly over previous SIMS O-isotope analytical locations to ensure the same chemical/age domain was analysed. Careful documentation of the CL images allowed for accurate laser targeting. Following two cleaning pulses and a 40s period of background analysis, samples were spot ablated for 40 s at a 10Hz repetition rate using a 50 µm beam (for >90% of analyses and a 32 µm beam for the <10% of smaller grains or grains with internal complexity like large inherited cores or thick metamorphic rims) and laser energy at the sample surface of 2.8-3.0 J cm^{-2}. An additional 15 s of baseline was collected after ablation. The sample cell was flushed with ultrahigh purity He (320 mL min^{-1}) and N_2 (1.2 mL min^{-1}) and high purity Ar was employed as the plasma carrier gas, split to each mass spectrometer.

For Hf isotope analysis, all isotopes (^{180}Hf, ^{179}Hf, ^{178}Hf, ^{177}Hf, ^{176}Hf, ^{175}Lu, ^{174}Hf, ^{173}Yb, ^{172}Yb and ^{171}Yb) were counted on the Faraday collector array. Time resolved data was baseline subtracted and reduced using Iolite v3.71 (Paton et al. 2011; DRS after Woodhead et al., 2004), where ^{176}Yb and ^{176}Lu were removed from the 176 mass signal using ^{176}Yb/^{173}Yb = 0.7962 and ^{176}Lu/^{175}Lu = 0.02655 with an exponential law mass bias correction assuming ^{172}Yb/^{173}Yb = 1.35274 (from Chu et al. 2002). The interference corrected ^{176}Hf/^{177}Hf was normalized to ^{179}Hf/^{177}Hf = 0.7325 (from Patchett and Tatsumoto 1980) for mass bias correction. An effective ^{176}Yb/^{173}Yb correction factor was determined for each session by iteratively adjusting the ^{176}Yb/^{173}Yb ratio until standard corrected ratios on secondary zircon reference materials with varying Yb content yielded values within the recommended range. No correlation was apparent between the abundance of interfering isotopes (Yb or Lu) and corrected ^{176}Hf/^{177}Hf ratios. Zircons from the Mud Tank carbonatite locality (Woodhead and Hergt 2005) were analysed together with the samples in each session to monitor the accuracy of the results with FC1, 91500 and Plešovice zircons included as secondary standards. All yielded weighted averages within uncertainty of their accepted values (Mud Tank ^{176}Hf/^{177}Hf = 0.282507 ± 0.000004; FC1 ^{176}Hf/^{177}Hf = 0.282158 ± 0.000005; 91500 ^{176}Hf/^{177}Hf = 0.282294 ± 0.000004; Plešovice ^{176}Hf/^{177}Hf = 0.282472 ± 0.000003) (Wiedenbeck et al. 2004; Slama et al. 2008). All data for primary and secondary reference standards is presented in Supplementary Table S4). In addition, the corrected ^{180}Hf/^{177}Hf ratio was calculated to monitor the accuracy of the mass bias correction and yielded an average value of 1.886864 ± 15 (MSWD = 0.59), which is within the range of values reported by Thirlwall and Anczkiewicz (2004). For a representative analysis of the laser signal, see raw data for a single analysis of the Mud Tanks reference zircon in Supplementary Table S6. All raw published and unpublished Lu/Hf isotopic data for individual zircon grains from previous studies has been recalculated for $\varepsilon_{Hf}(t)$ and $T_{(DM)}$ ages using the exact same parameters as the new data collected in this study to ensure consistency throughout the datasets. CHUR parameters (^{176}Hf/^{177}Hf = 0.282785, ^{176}Lu/^{177}Hf = 0.033600) from Bouvier et al. (2008) and a λ^{176}Lu decay constant of 1.867 x 10^{-11} y^{-1} (Soderlund et al. 2004) were used to calculate $\varepsilon_{Hf}(t)$ values and ^{176}Hf/^{177}Hf ratios. Model ages ($T_{(DM)}$) for zircons were calculated using individual spot ^{206}Pb/^{238}U ages (obtained simultaneously from the same volume of zircon used for Lu/Hf isotopic analysis; for some published analyses, the granitoid ^{206}Pb/^{238}U age was used as the spot ^{206}Pb/^{238}U age was unavailable), initial ^{176}Hf/^{177}Hf ratios and a Bulk Earth ^{176}Lu/^{177}Hf ratio of 0.015 (Goodge and Vervoort 2006). Hf isotopic evolution of the depleted mantle (DM) was determined using ^{176}Lu/^{177}Hf$_{DM}$ = 0.038512 and ^{176}Hf/^{177}Hf$_{DM}$ = 0.283225 (Vervoort and Blichert-Toft 1999). There are many assumptions and inherent uncertainties with respect to the calculated zircon model ages ($T_{(DM)}$) presented (i.e., Faure and Mensing 2005); however, given the broad range of model ages for zircon from the EID (c. 1300 – 500 Ma), any uncertainties associated with model age calculations will not change the conclusion that the age of the underlying source is directly related to mantle melting and hydrothermal alteration associated with Rodinia assembly (1300 – 900 Ma) and rifting (800 – 500 Ma).

For the Q-ICP-MS U-Pb analysis, the following isotopes were monitored: ^{202}Hg, ^{204}Pb, ^{206}Pb, ^{207}Pb, ^{208}Pb (0.1 s dwell time on all Pb isotopes), ^{232}Th, and ^{238}U (0.025 s dwell time on U and Th). The primary dating reference materials used in this study were 91500 (1062.4±0.4 Ma; Wiedenbeck et al. 2004) and OG1 (3465.4±0.6; Stern et al. 2009) with Plešovice (337.13±0.37 Ma; Slama et al. 2008) and GJ-1 (608.53±0.37; Jackson et al. 2004) analysed as secondary age standards. ^{206}Pb/^{238}U ages and ^{207}Pb/^{206}Pb calculated for zircon age standards, treated as unknowns, were found to be within 2% of the accepted value. The time-resolved mass spectra were reduced using the U_Pb_Geochronology4 data reduction scheme in Iolite 3.71 (Paton et al. 2011).

References

Allibone, A.H., and Tulloch, A.J., 2004, Geology of the plutonic basement rocks of Stewart Island, New Zealand: New Zealand Journal of Geology and Geophysics, v. 47, p. 233–256.

Allibone, A.H., MacKenzie, D., Turnbull, R., Tulloch, A., and Craw, D., 2016a, Polymetallic mineralisation associated with Carboniferous I-type granitoids in central Stewart Island, New Zealand: New Zealand Journal of Geology and Geophysics, v. 59, p. 436–456.

Allibone, A.H., MacKenzie, D., Turnbull, R., Tulloch, A., Craw, D., and Palin, M., 2016b, Polymetallic mineralised veins in ferroan/A-type Cretaceous leucogranite, Stewart Island, New Zealand: New Zealand Journal of Geology and Geophysics, v. 59, p. 457–474.

Black, L.P., Kamo, S.L., Allen, C.M., Davis, D.W., Aleinikoff, J.N., Valley, J.W., Mundil, R., Campbell, I.H., Korsch, R.J., Williams, I.S., and Foudoulis, C., 2004, Improved ^{206}Pb/^{238}U microprobe geochronology by the monitoring of a trace-element-related matrix effect; SHRIMP, ID-TIMS, ELA-ICP-MS and oxygen isotope documentation for a series of zircon standards: Chemical Geology, v. 205, p. 115–140.

Bouvier, A., Vervoort, J.D., and Patchett, P.J., 2008, The Lu-Hf and Sm-Nd isotopic composition of CHUR: constraints from unequilibrated chondrites and implications for the bulk composition of terrestrial planets: Earth and Planetary Science Letters, v. 273, p. 48–57.

Buritica, L.F., Schwartz, J.J., Klepeis, K.A., Miranda, E.A., Tulloch, A.J., Coble, M.A., Kylander-Clark, A.R., 2019, Temporal and spatial variations in magmatism and transpression in a Cretaceous arc, Median Batholith, Fiordland, New Zealand: Lithosphere, v. 11, p. 652–682.

Chu, N.-C., Taylor, R. N., Chavagnac, V., Nesbitt, R. W., Boella, R. M., Milton, J. A., German, C. R., Bayon, G., and Burton, K., 2002, Hf isotope ratio analysis using multi-collector inductively coupled plasma mass spectrometry: an evaluation of isobaric interference corrections: Journal of Analytical Atomic Spectrometry, v. 17, p. 1567-1574.

Davids, C., 1999, A thermochronological study of southern Fiordland, New Zealand. Unpublished PhD thesis, Geology Department, Australian National University, Canberra.

Decker, M., 2016, Triggering mechanisms for a magmatic flare-up of the lower crust in Fiordland, New Zealand, from U–Pb zircon geochronology and O–Hf zircon geochemistry. MS thesis, California State University Northridge, 122 pp.

Faure, G., Mensing, T.M., 2005, Isotopes - principles and applications. John Wiley & Sons, Inc, 897 p.

Goodge, J.W., and Vervoort, J.D., 2006, Origin of Mesoproterozoic A-type granites in Laurentia: Hf isotope evidence: Earth and Planetary Science Letters, v. 243, p. 711–731.

Jackson, S.E., Pearson, N.J., Griffin, W.L., and Belousova, E.A., 2004, The application of laser ablation-inductively coupled-mass spectrometry to in situ U-Pb zircon geochronology: Chemical Geology, v. 211, p. 47-69.

Kimbrough, D.L., Tulloch, A.J., Coombs, D.S., Landis, C.A., Johnston, M.R., and Mattinson, J.M., 1994, Uranium-lead zircon ages from the Median Tectonic Zone, New Zealand: New Zealand Journal of Geology and Geophysics, v. 37, p. 393–419.

Kita, N.T., Ushikubo, T., Fu, B., and Valley, J.W., 2009, High precision SIMS oxygen isotope analysis and the effect of sample topography: Chemical Geology, v. 264, p. 43–57.

Klepeis, K.A., Clarke, G.L., Gehrels, G., and Vervoort, J., 2004, Processes controlling vertical coupling and decoupling between the upper and lower crust orogens: results from Fiordland, New Zealand: Journal of Structural Geology, v. 26, p. 765–791.

Muir, R.J., Ireland, T.R., Weaver, S.D., and Bradshaw, J.D., 1996, Ion microprobe dating of Paleozoic granitoids: Devonian magmatism in New Zealand and correlations with Australia and Antarctica: Chemical Geology, v. 127, p. 191–210.

Muir, R.J., Ireland, T.R., Weaver, S.D., Bradshaw, J.D., Waight, T.E., Jongens, R., and Eby, N., 1997, SHRIMP U-Pb geochronology of Cretaceous magmatism in northwest Nelson-Westland, South Island, New Zealand: New Zealand Journal of Geology and Geophysics, v. 40, p. 453–463.

Muir, R.J., Ireland, T.R., Weaver, S.D., Bradshaw, J.D., Evans, J.A., Eby, G.N., and Shelley, D., 1998, Geochronology and geochemistry of a Mesozoic magmatic arc system, Fiordland, New Zealand: Journal of the Geological Society, London, v. 155, p. 1037–1053.

Patchett, P. J., and Tatsumoto, M., 1980, Hafnium isotope variations in oceanic basalts: Geophysical Research Letters, v. 7, p. 1077–1080.

Paton, C., Hellstrom, J., Bence, P., Woodhead, J., and Hergt, J., 2011, Iolite: Freeware for the visualisation and processing of mass spectrometric data: Journal of Analytical and Atomic Spectrometry, v. 26, p. 2508–2518.

Peck, H.W., Valley, J.W., Wilde, S.A., and Graham, C.M., 2001, Oxygen isotope ratios and rare earth elements in 3.3 to 4.4 Ga zircons: Ion microprobe evidence for high ó^{18}O continental crust and oceans in the Early Archean: Geochimica at Cosmochimica Acta, v. 65, p. 4215–4229.

Ramezani, J., and Tulloch, A.J., 2009, TIMS U-Pb geochronology of southern and eastern Fiordland. Lower Hutt: Institute of Geological and Nuclear Sciences. http://data.gns.cri.nz/paperdata/index.jsp.

Ringwood, M.F., Schwartz, J.J., Turnbull, R.E., and Tulloch, A.J., *IN REVIEW*, Lower plate controls on Phanerozoic arc magmatic tempos in the Zealandia Cordillera: Geology.

Sagar, M.W., Palin, J.M., Tulloch, A.J., and Heath, L.A., 2016, The geology, geochronology and affiliation of the Glenroy Complex and adjacent plutonic rocks, southeast Nelson: New Zealand Journal of Geology and Geophysics, v. 59, p. 213–235.

Schwartz, J.J., Andico, S., Turnbull, R.E., Klepeis, K.A., Tulloch, A.J., Kitajima, K., and Valley, J.W., 2020, Crustal and Isotopic Architecture of the Median Batholith, Fiordland, New Zealand. American Mineralogist: (in press) https://doi.org/10.2138/am-2021-7626.

Scott, J.M., Cooper, A.F., Palin, J.M., Tulloch, A.J., Kula, J., Jongens, R., and Spell, T.L., 2009, Tracking the influence of a continental margin on growth of a magmatic arc, Fiordland, New Zealand, using thermobarometry, thermochronology, and zircon U-Pb and Hf isotopes: Tectonics, v. 28(6).

Slama, J., Kosler, J., Condon, D.J., Crowley, J.L., Gerdes, A., Hanchar, J.M., Horstwood, M.S.A., Morris, G.A., Nasdala, L., Norberg, N., Schaltegger, U., Schoene, B., Tubrett, M.N., and Whitehouse, M.J., 2008, Plesovice zircon – A new natural reference material fo U-Pb and Hf isotopic microanalysis: Chemical Geology, v. 249, p. 1–35.

Soderlund, U., Patchett, P.J., Vervoort, J.D., and Isachsen, C.E., 2004, The Lu-176 decay constant determined by Lu-Hf and U-Pb isotope systematics of Precambrian mafic intrusions: Earth and Planetary Science Letters, v. 219, p. 311–324.

Spencer, C.J., Cavosie, A.J., Raub, T.D., Roloinson, H., Jeon, H., Searle, M.P., Miller, J.A., McDonald, B.J., and Evans, N.J., 2017, Evidence for melting mud in Earth's mantle from extreme oxygen isotope signatures in zircon: Geology, v. 45, p. 975–978.

Stern, R.A., Bodorkos, S., Kamo, S.L., Hickman, A.H., and Corfu, F., 2009, Measurement of SIMS instrumental mass fractionation of Pb isotopes during zircon dating: Geostandards and Geoanalytical Research, v. 33, p. 145–168.

Strong, D.T., Turnbull, R.E., Haubrock, S., and Mortimer, N., 2016, Petlab: New Zealand's national rock catalogue and geoanalytical database: New Zealand Journal of Geology and Geophysics, v. 59, p. 475–481.

Thirlwall, M., and Anczkiewicz, R., 2004, Multidynamic isotope ratio analysis using MC–ICP–MS and the causes of secular drift in Hf, Nd and Pb isotope ratios: International Journal of Mass Spectrometry, v. 235, p. 59–81.

Tulloch, A.J., Ireland, T.R., Kimbrough, D.L., Griffin, W.L., and Ramezani, J., 2011, Autochthonous inheritance of zircon through Cretaceous partial melting of Carboniferous plutons: The Arthur River Complex, Fiordland, New Zealand: Contributions to Mineralogy and Petrology, v. 161, p. 401–421.

Tulloch, A.J., Ramezani, J., Kimbrough, D.L., Faure, K., and Allibone, A.H., 2009, U-Pb geochronology of mid-Paleozoic plutonism in western New Zealand: Implications for S-type granite generation and growth of the east Gondwana margin: GSA Bulletin, v. 121, p. 1236–1261.

Turnbull, R., Tulloch, A., Ramezani, J., Jongens, R., 2016, Extension-facilitated pulsed SIA-type "flare-up" magmatism at 370 Ma along the southeast Gondwana margin in New Zealand: insights from U-Pb geochronology and geochemistry: GSA Bulletin, v. 128, p. 1500–1520.

Vervoort, J.D., and Blichert-Toft, J., 1999, Evolution of the depleted mantle: Hf isotope evidence from juvenile rocks through time: Geochimica et cosmochimica acta, v. 63, p. 533–556.

Wiedenbeck, M., Hanchar, J.M., Peck, W.H., Sylvester, P., Valley, J., Whitehouse, M., Kronz, A., Morishita, Y., Nasdala, L., Fiebig, J., and Franchi, I., 2004, Further characterisation of the 91500 zircon crystal: Geostandards and Geoanalytical Research, v. 28, p. 9–39.

Woodhead, J.D., and Hergt, J.M., 2005, A preliminary appraisal of seven natural zircon reference materials for in situ Hf isotope determination: Geostandards and Geoanalytical Research, v. 29, p. 183–195.

Woodhead, J., Hergt, J., Shelley, M., Eggins, S., and Kemp, R., 2004, Zircon Hf-isotope analysis analysis with an excimer laser, depth profiling, ablation of complex geometries and comcomitant age estimation: Chemical Geology, v. 209, p. 121–135.

SUPPLEMENTAL FILES

Supplementary Figure S1. Representative cathodoluminescence (CL) image of zircon from sample P76172. O-isotope analysis was completed first using CL and transmitted light images of zircon grains as a guide to spot location. U-Pb-Lu-Hf analyses were completed on top of the O-isotope spot localities.

Supplementary Figure S2. Individual zircon analyses highlighting zircon fractionation indexes for (A) $\delta^{18}O_{zircon}$ versus whole-rock SiO_2 composition of the host granitoid, and (B) $\delta^{18}O_{zircon}$ versus Zr/Hf in zircon. No correlations are observed indicating that the variability observed in zircon O- and Hf-isotope compositions are not controlled by fractional crystallization processes. (C) simplified geological map outlining the extent, age and type (I, S, A) of Phanerozoic plutonic rocks that intrude early Paleozoic sedimentary terranes in New Zealand.

Supplementary Figure S3. Average O- and Hf-isotopic compositions for each pluton for which multiple zircon analyses were completed. The isotopic homogeneity of the eastern isotopic domain relative to the western isotopic domain is apparent.

Supplementary Figure S4. Individual spot analyses for (A) $\varepsilon_{Hf}(T)$ and (B) $\delta^{18}O$ zircon values plotted against the U-Pb age obtained for each spot. All analyses were performed on the same spot locality on the zircon grain.

Supplementary Table S1. O-isotope data for all individual zircon spot analyses from Zealandia plutonic rocks.

Supplementary Table S2. Lu-Hf isotopic data and $^{206}Pb/^{238}U$ age for all individual zircon spot analyses from Zealandia plutonic rocks.

Supplementary Table S3. O-isotope data for all standard reference materials analyzed during O-isotope SIMS analysis.

Supplementary Table S4. Lu-Hf isotopic data for all standard reference materials analyzed during Hf-isotope LA-MC-ICPMS analysis.

Supplementary Table S5. Sample location information

Supplementary Table S6. Example of laser output for a single Mud Tank reference zircon, analyzed on 24 May 2019.

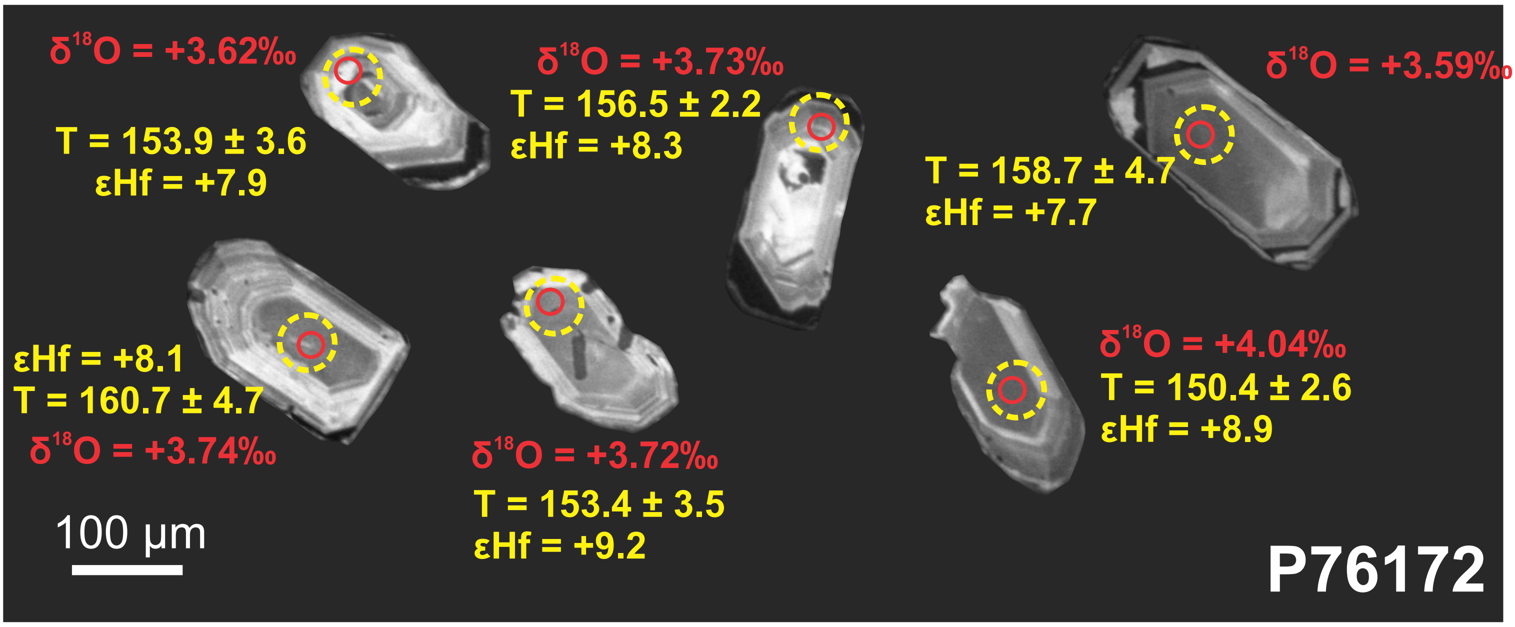

Supplementary Figure S1. Representative Cathodoluminescence (CL) image of zircon from sample P76172. O-isotope analysis was completed first using CL and transmitted light images of zircon grains as a guide to spot location. U-Pb-Lu-Hf analyses were completed on top of the O-isotope spot localities.

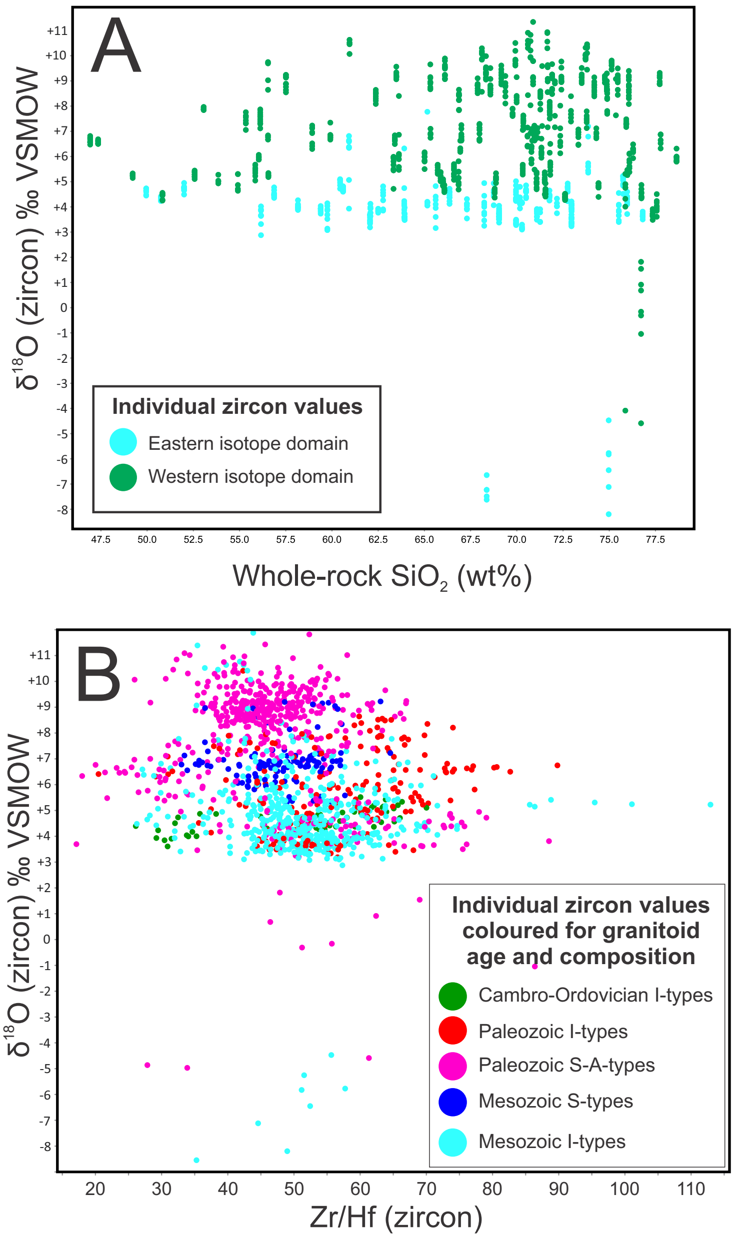

Supplementary Figure S2. Individual zircon anaylses highlighting zircon fractionation indexes for (A) $\delta^{18}O_{zircon}$ versus whole-rock SiO_2 composition of the host granitoid, and (B) $\delta^{18}O_{zircon}$ versus Zr/Hf in zircon. No correlations are observed indicating that the variability observed in zircon O- and Hf-isotopic compositions are not controlled by fractional crystallisation processes. (C) Simplified geological map outlining the extent, age and type (I, S, A) of Phanerozoic granitoids that intrude early Paleozoic sedimentary terranes in New Zealand.

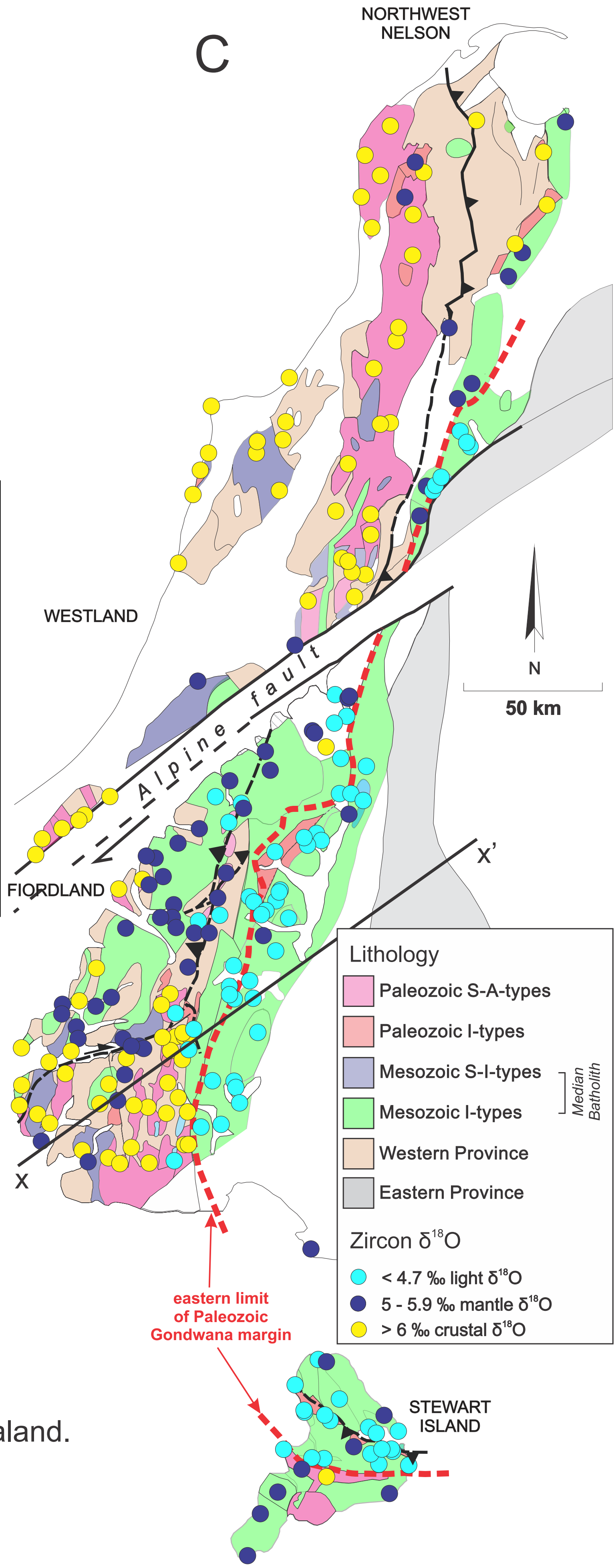

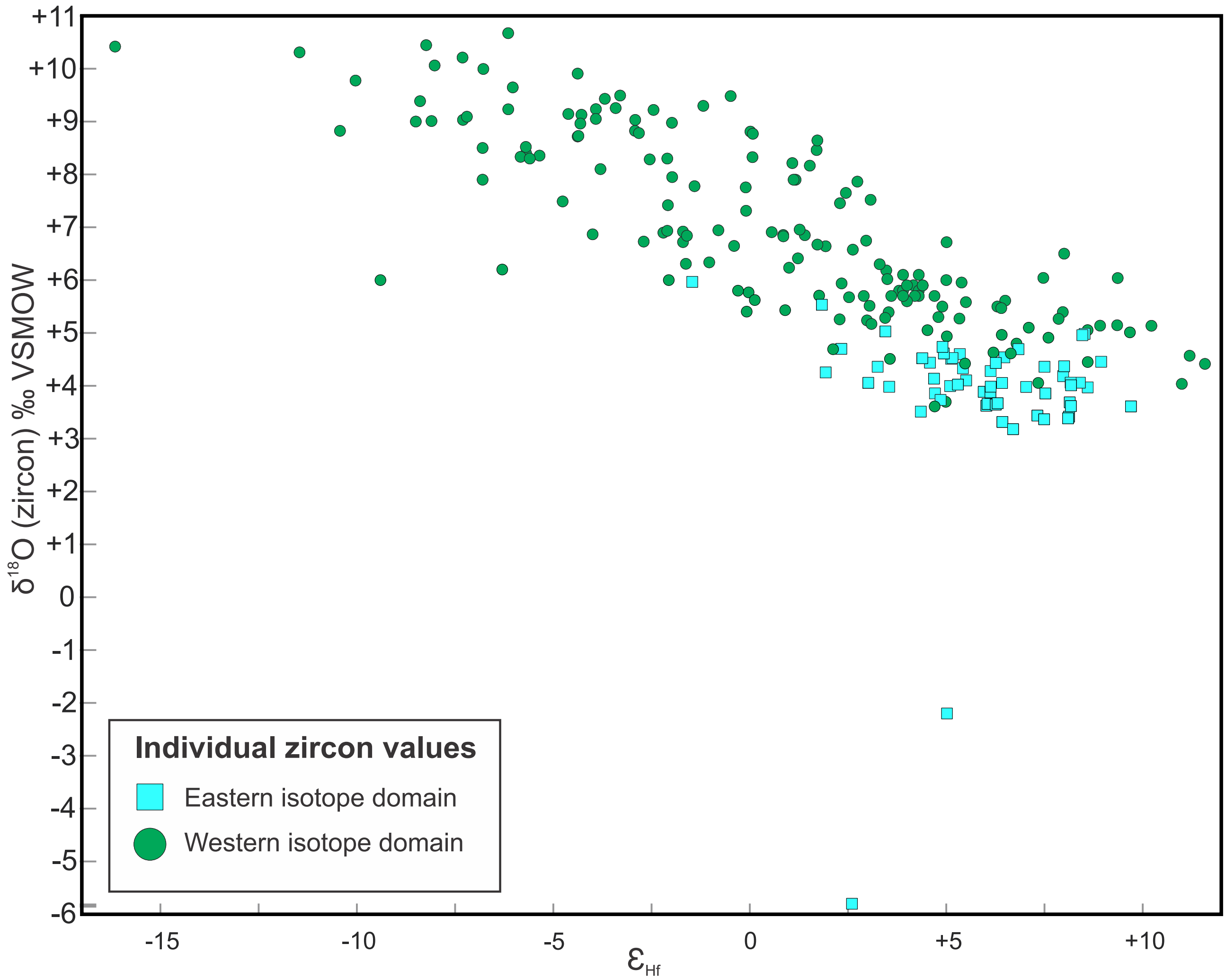

Supplementary Figure S3. Average O- and Hf-isotopic compositions for each pluton for which multiple zircon analyses were completed. The isotopic homogeneity of the eastern isotopic domain relative to the western isotopic domain is apparent.

Supplementary Figure S4. Individual spot analyses for (A) εHf(T) and (B) $\delta^{18}O$ zircon values plotted against the U-Pb age obtained for each spot. All analyses were performed on the same spot locality on the zircon grain.